


Magnetic order transition in monolayer MoS₂ induced by strong intervalley correlationPeng Fan^{1,2} and Zhen-Gang Zhu^{2,1,3,*}¹*Theoretical Condensed Matter Physics and Computational Materials Physics Laboratory, College of Physical Sciences, University of Chinese Academy of Sciences, Beijing 100049, China*²*School of Electronic, Electrical and Communication Engineering, University of Chinese Academy of Sciences, Beijing 100049, China*³*CAS Center for Excellence in Topological Quantum Computation, University of Chinese Academy of Sciences, Beijing 100190, China* (Received 2 June 2021; revised 4 November 2021; accepted 4 November 2021; published 16 November 2021)

In this paper, we study a model for monolayer molybdenum disulfide, including the intravalley and intervalley electron-electron interaction. We solve the model at a self-consistent mean-field level and get three solutions: L_0 , L_+ , and L_- . As for L_0 , the spin polarizations are opposite at \mathbf{K} and \mathbf{K}' valleys and the total magnetization is zero. L_{\pm} describes two degenerate spin-polarized states, and the directions of polarization are opposite for the states of L_+ and L_- . Based on these results, the ground state can be deduced to be spin polarized in domains in which their particular states can be randomly described by L_+ or L_- . Therefore, a zero net magnetization is induced for zero external magnetic field \mathbf{B} , but a global ferromagnetic ground state for a nonzero \mathbf{B} . We estimate the size of domains as several nanometers. With the increase of the chemical potential, the ground state changes between L_0 and L_{\pm} , indicating first-order phase transitions at the borders, which is coincident with the observation of photoluminescence experiments in the absence of the external magnetic field [J. G. Roch, *et al.*, *Phys. Rev. Lett.* **124**, 187602 (2020)].

DOI: [10.1103/PhysRevB.104.195417](https://doi.org/10.1103/PhysRevB.104.195417)**I. INTRODUCTION**

Transition-metal dichalcogenides (TMDCs) [1,2] are a class of materials of the type MX_2 , where M is a transition-metal atom (Mo, W, V, Hf, etc.) and X is a chalcogen atom (S, Se, Te, etc.). In recent decades, interest has grown rapidly in TMDCs due to their impressive electronic [1,3–7], optical [2,3], and mechanical properties [8], and the broad application to electronics [9–11], spintronics [12,13], valleytronics [14,15], optoelectronics [2,16], and sensing [17]. When bulk TMDCs are thinned to monolayers, correlation effects become much more important than that in the bulk, because the three-dimensional Coulomb interaction is only screened in two dimensions, which results in a weak dielectric screening [18]. Many experiments have demonstrated the existence of strong electron-electron (e - e) interaction in monolayer TMDCs (ML-TMDCs), including interaction-induced giant paramagnetic (PM) response in ML-MoSe₂ [19], biexciton photoluminescence peaks in ML-WX₂ ($X = S, Se$) [20,21], enhanced valley magnetic response, and quantum Hall states sequence transition in ML-WSe₂ [22,23]. Optical susceptibility measurements of the molybdenum disulfide (MoS₂) monolayer in van der Waals heterostructures provided by Roch *et al.* show that e - e interactions, especially the intervalley exchange interaction, result in a first-order phase transition from a spin-unpolarized ground state to a spin-polarized state in the presence of an external magnetic field \mathbf{B} [24–26]. In the photoluminescence spectrum, an abrupt change marks this first-order phase transition when the trion peak (X^-) evolves into the Mahan exciton peak (Q) [25]. This first-order phase transition attributes to the nonanalytic correction in the free

energy [25,27]. Without \mathbf{B} , the same abrupt change is still observed, which implies that a magnetic order transition occurs like the case of nonzero \mathbf{B} [25]. However, the total magnetization is zero in the whole process, which seems to indicate that the transition of the magnetic order doesn't occur. It is confusing. Roch *et al.* [25] proposed that the fluctuation between “puddles” of the spin up and spin down leads to the zero total magnetization at low electron density. However, there is no theoretical demonstration of the puddles (the degenerate spin-polarized states). In previous theoretical studies [28,29] intervalley e - e interaction was ignored and the spin-spin couplings in the intravalley and intervalley were not appreciated, which play a vital role, as shown by our results, in determining the properties of the ground state. We are motivated by the zero magnetic field experimental observations and the lack of theoretical explanation. Therefore, we focus on this case and try to understand the peculiar observations in experiments. In this paper, we study a model for ML-MoS₂, including the intravalley and intervalley Coulomb interaction, based on the low-energy noninteracting Hamiltonian derived in previous studies [13] and develop a self-consistent mean-field method, emphasizing the effective intervalley spin-spin couplings. It is found that the ground state is composed of two degenerated spin-polarized states at a certain electron density, giving rise to a zero total magnetization. By tuning the electron density via the chemical potential, a first-order phase transition occurs between the unpolarized state to the spin-polarized states, which is consistent with the experiment [25].

II. THE MODEL AND SELF-CONSISTENT CALCULATION PROCEDURE

Figure 1 shows the crystal structure of ML-MoS₂ and its first Brillouin zone (BZ) [30]. The minima of the conduction

*zgzhu@ucas.ac.cn

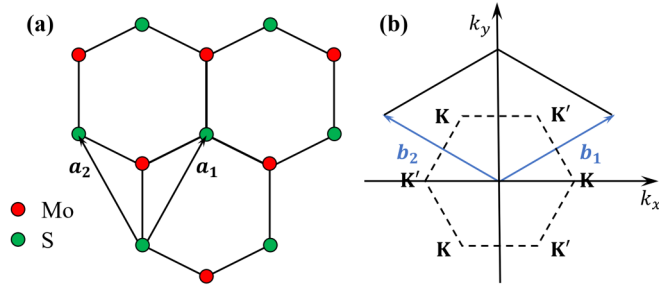


FIG. 1. (a) Honeycomb lattice of the monolayer MoS₂. The red dot is Mo and the green dot is S. \mathbf{a}_1 and \mathbf{a}_2 are the primitive vectors. (b) Brillouin zone (BZ) of the honeycomb lattice. \mathbf{b}_1 and \mathbf{b}_2 are the primitive vectors of the reciprocal lattice.

band are located at the corners (\mathbf{K} , \mathbf{K}'). For the description of the noninteracting case, we use the effective Hamiltonian of ML-MoS₂ around the Dirac cones [13,31] as

$$\hat{H}_0 = at(\tau k_x \sigma_x + k_y \sigma_y) + \frac{\Delta}{2} \sigma_z - \lambda \tau \frac{\sigma_z - 1}{2} \hat{s}_z, \quad (1)$$

where $\tau = \pm 1$ are valley indexes for \mathbf{K} and \mathbf{K}' (see Fig. 1). The spin splitting caused by spin-orbit coupling is 2λ . σ_α ($\alpha = x, y, z$) are the Pauli matrices. a is the lattice constant. t is the hopping integral. Δ is the energy gap between the conduction band and valence band (when $\lambda = 0$). \hat{s}_z is the z component of the spin operator. For convenience, BZ is chosen as the diamond region in the following calculation [see Fig. 1(b)]. The energy eigenvalues of the Hamiltonian are [32]

$$E_{n\tau s} = \lambda \tau s / 2 \pm \sqrt{(atk)^2 + [(\Delta - \lambda \tau s) / 2]^2}, \quad (2)$$

where $s = \pm 1$ are the spin indexes for spin up and down, respectively. The up plus (bottom minus) sign in Eq. (2) denotes the conduction (valence) band [c (v)]. k is the module of the wave vector. The corresponding eigenstates are denoted as $|n\tau ks\rangle$, where $n = c$ or v .

The Coulomb interaction between electrons is

$$V(\mathbf{r}_1 - \mathbf{r}_2) = \frac{e^2}{4\pi\epsilon_0} \frac{1}{|\mathbf{r}_1 - \mathbf{r}_2|}, \quad (3)$$

where e is the elementary charge and ϵ_0 is the vacuum permittivity. It is secondly quantized in the $|n\tau ks\rangle$ representation [33],

$$\hat{V} = \frac{1}{N} \sum_{s_1 s_2} \sum_{\mathbf{k}_1 \mathbf{k}_2} \sum_{\mathbf{k}_3 \mathbf{k}_4} n_1 n_2 n_3 n_4 \times \sum_{\tau_1 \tau_2 \tau_3 \tau_4} V_{\text{int}} a_{\mathbf{k}_1 s_1}^{n_1 \tau_1 \dagger} a_{\mathbf{k}_2 s_2}^{n_2 \tau_2 \dagger} a_{\mathbf{k}_3 s_3}^{n_3 \tau_3} a_{\mathbf{k}_4 s_4}^{n_4 \tau_4}, \quad (4)$$

where V_{int} denotes the strength of the e - e interaction and N is the number of unit cells. $a_{\mathbf{k}s}^{n\tau\dagger}$ ($a_{\mathbf{k}s}^{n\tau}$) is the creation (annihilation) operator in $|n\tau ks\rangle$ state. There are three kinds of e - e interaction: interaction between the conduction electrons, interaction between the valence electrons, and the interaction between the conduction electrons and the valence electrons. Here, we only take the interaction between the conduction electrons into consideration and eliminate the letter c , which is used to mark the conduction band, in the following formulas

for convenience. The strength of the e - e interaction in the conduction band is written as

$$V_{\text{int}} = \frac{1}{2N} \langle \tau_1 \mathbf{k}_1 s_1, \tau_2 \mathbf{k}_2 s_2 | V(\mathbf{r}_1 - \mathbf{r}_2) | \tau_4 \mathbf{k}_4 s_1, \tau_3 \mathbf{k}_3 s_2 \rangle. \quad (5)$$

\hat{V} in Eq. (A37) is thus expanded explicitly and approximated as

$$\hat{V} \approx \hat{V}_{\text{intra}} + \hat{V}_{\text{inter}}, \quad (6)$$

where

$$\hat{V}_{\text{intra}} = \frac{1}{N} \sum_{\mathbf{k}_1 \mathbf{k}_2} \sum_{\tau s} U a_{\mathbf{k}_1 s}^{\tau\dagger} a_{\mathbf{k}_2 s}^{\tau\dagger} a_{\mathbf{k}_2 s}^{\tau} a_{\mathbf{k}_1 s}^{\tau}, \quad (7)$$

$$\hat{V}_{\text{inter}} = \frac{1}{N} \sum_{\mathbf{k}_1 \mathbf{k}_2} \sum_{\tau s_1 s_2} U' a_{\mathbf{k}_1 s_1}^{\tau\dagger} a_{\mathbf{k}_2 s_2}^{\bar{\tau}\dagger} a_{\mathbf{k}_1 s_2}^{\tau} a_{\mathbf{k}_2 s_1}^{\bar{\tau}}. \quad (8)$$

\hat{V}_{intra} and \hat{V}_{inter} denote the intravalley and intervalley e - e interaction, respectively. U and U' are the strengths of the corresponding e - e interactions:

$$U = \frac{1}{2N} \langle \tau \mathbf{k}_1, \tau \mathbf{k}_2 | V(\mathbf{r}_1 - \mathbf{r}_2) | \tau \mathbf{k}_1, \tau \mathbf{k}_2 \rangle, \quad (9)$$

$$U' = \frac{1}{2N} \langle \tau \mathbf{k}_1, \bar{\tau} \bar{\mathbf{k}}_2 | V(\mathbf{r}_1 - \mathbf{r}_2) | \bar{\tau} \bar{\mathbf{k}}_2, \tau \mathbf{k}_1 \rangle. \quad (10)$$

$\bar{\tau}$ (\bar{s}) represents the opposite valley (spin) of τ (s). \mathbf{k} ($\bar{\mathbf{k}}$) indicates the relative wave vector with respect to the minimum of τ ($\bar{\tau}$) valley. Quantitatively, it has been estimated in the static screening limit that due to the small Bohr radius the intervalley e - e interaction is comparable to the intravalley interaction even at high electron density [26]. Hence, it is necessary to take the intervalley e - e interaction into consideration when one deals with the Coulomb interaction in TMDCs [26]. For the purpose of a qualitative discussion, U and U' are regarded as constants. Details of the above approximation are shown in Appendix A.

We apply the mean-field approximation (MFA) [33] to \hat{V}_{intra} and \hat{V}_{inter} , respectively. As for \hat{V}_{intra} , it reads

$$\hat{V}_{\text{intra}}^{\text{MF}} \approx \sum_{\mathbf{k}s} (U_{\tau s} a_{\mathbf{k}s}^{\tau\dagger} a_{\mathbf{k}s}^{\tau} + U_{\bar{\tau} s} a_{\mathbf{k}s}^{\bar{\tau}\dagger} a_{\mathbf{k}s}^{\bar{\tau}}), \quad (11)$$

where

$$U_{\tau s} = \frac{2}{N} \sum_{\mathbf{k}} U \langle n_{\mathbf{k}s}^{\tau} \rangle, \quad U_{\bar{\tau} s} = \frac{2}{N} \sum_{\mathbf{k}} U \langle n_{\mathbf{k}s}^{\bar{\tau}} \rangle. \quad (12)$$

$n_{\mathbf{k}s}^{\tau} = a_{\mathbf{k}s}^{\tau\dagger} a_{\mathbf{k}s}^{\tau}$ is the particle number operator. In this paper, we merely consider the zero temperature case. Therefore, $\langle \dots \rangle$ means the ground-state average. In terms of the spin operators, $S_{\tau\mathbf{k}}^z = \frac{1}{2}(n_{\mathbf{k}\uparrow}^{\tau} - n_{\mathbf{k}\downarrow}^{\tau})$, $S_{\tau\mathbf{k}}^+ = a_{\mathbf{k}\uparrow}^{\tau\dagger} a_{\mathbf{k}\downarrow}^{\tau}$, and $S_{\tau\mathbf{k}}^- = a_{\mathbf{k}\downarrow}^{\tau\dagger} a_{\mathbf{k}\uparrow}^{\tau}$, \hat{V}_{inter} is rewritten as

$$\hat{V}_{\text{inter}} = -\frac{U'}{N} \sum_{\mathbf{k}_1 \mathbf{k}_2} (n_{\mathbf{k}_1}^{\tau} n_{\mathbf{k}_2}^{\bar{\tau}} + 4\mathbf{S}_{\tau\mathbf{k}_1} \cdot \mathbf{S}_{\bar{\tau}\mathbf{k}_2}), \quad (13)$$

where $n_{\mathbf{k}}^{\tau} = \sum_s n_{\mathbf{k}s}^{\tau}$. \mathbf{S} is the spin operator and

$$\mathbf{S}_{\tau\mathbf{k}_1} \cdot \mathbf{S}_{\bar{\tau}\mathbf{k}_2} = S_{\tau\mathbf{k}_1}^z S_{\bar{\tau}\mathbf{k}_2}^z + \frac{1}{2}(S_{\tau\mathbf{k}_1}^+ S_{\bar{\tau}\mathbf{k}_2}^- + S_{\tau\mathbf{k}_1}^- S_{\bar{\tau}\mathbf{k}_2}^+). \quad (14)$$

In Eq. (13), the first and second terms give the intervalley density-density interaction and the intervalley spin-spin cou-

pling. We apply the MFA to Eq. (13) and obtain

$$\hat{V}_{\text{inter}}^{\text{MF}} \approx - \sum_k (U'_\tau n_{\bar{k}}^\tau + U'_\tau n_{\bar{k}}^\tau + \mathbb{M}_{\bar{\tau}} S_{\bar{k}}^z + \mathbb{M}_\tau S_{\tau k}^z), \quad (15)$$

where

$$U'_{\bar{\tau}(\tau)} = \frac{1}{N} \sum_{\mathbf{k}(\bar{\mathbf{k}})} U' \langle n_{\mathbf{k}(\bar{\mathbf{k}})}^{\tau(\bar{\tau})} \rangle, \quad \mathbb{M}_{\bar{\tau}(\tau)} = \frac{4}{N} \sum_{\mathbf{k}(\bar{\mathbf{k}})} U' \langle S_{\tau \mathbf{k}(\bar{\tau} \bar{\mathbf{k}})}^z \rangle.$$

In Eq. (13), the direction of \mathbf{S} is chosen as the z axis. By defining

$$\mathbb{X}_{\tau s} = U'_\tau + \frac{1}{2} s \mathbb{M}_\tau, \quad \mathbb{X}_{\bar{\tau} s} = U'_{\bar{\tau}} + \frac{1}{2} s \mathbb{M}_{\bar{\tau}}, \quad (16)$$

where $s = \pm 1$ for states with spins parallel and antiparallel to the \mathbf{S} , we obtain

$$\hat{V}_{\text{inter}}^{\text{MF}} \approx - \sum_{ks} (\mathbb{X}_{\tau s} a_{ks}^{\tau\dagger} a_{ks}^\tau + \mathbb{X}_{\bar{\tau} s} a_{ks}^{\bar{\tau}\dagger} a_{ks}^{\bar{\tau}}). \quad (17)$$

Therefore, the MFA of the interaction, i.e., $\hat{V}_{\text{MF}} = \hat{V}_{\text{intra}}^{\text{MF}} + \hat{V}_{\text{inter}}^{\text{MF}}$, is

$$\hat{V}_{\text{MF}} = \sum_{ks} (\mathbb{F}_{\tau s} a_{ks}^{\tau\dagger} a_{ks}^\tau + \mathbb{F}_{\bar{\tau} s} a_{ks}^{\bar{\tau}\dagger} a_{ks}^{\bar{\tau}}). \quad (18)$$

$\mathbb{F}_{\tau s}$ and $\mathbb{F}_{\bar{\tau} s}$ are the effective mean fields, which read

$$\mathbb{F}_{\tau s} = \mathbb{U}_{\tau s} - \mathbb{X}_{\tau s}, \quad \mathbb{F}_{\bar{\tau} s} = \mathbb{U}_{\bar{\tau} s} - \mathbb{X}_{\bar{\tau} s}. \quad (19)$$

The total mean-field Hamiltonian reads

$$\mathbb{H}_{\text{total}}^{\text{MF}} = \sum_{ks} (\mathbb{E}_{c\tau s}(\mathbf{k}) a_{ks}^{\tau\dagger} a_{ks}^\tau + \mathbb{E}_{c\bar{\tau} s}(\bar{\mathbf{k}}) a_{ks}^{\bar{\tau}\dagger} a_{ks}^{\bar{\tau}}), \quad (20)$$

where the energy spectrum

$$\mathbb{E}_{c\tau(\bar{\tau})s}(\mathbf{k}) = E_{c\tau(\bar{\tau})s}(\mathbf{k}) + \mathbb{F}_{\tau(\bar{\tau})s} - \mu, \quad (21)$$

where μ is the chemical potential. In above MFA, we omit the constant terms, which do not affect our general discussions and qualitative conclusions. The constant terms neglected in the calculations merely shift all energy bands simultaneously. This leads us to a zero-energy redefinition. This shift cannot affect the determination of the solutions which are determined by the parameters that are not entangled with the absolute energies but the relative energy with respect to the zero energy. It is easy then to calculate the free energy:

$$E_{\text{free}} = \sum_{\tau s} \int \mathbb{E}_{c\tau s}(\mathbf{k}) d\mathbf{k}. \quad (22)$$

The detailed calculations of E_{free} can be found in Appendix C. To calculate the effective mean fields, averages $\langle n_{ks}^\tau \rangle$ need to be calculated. We thus introduce

$$\tilde{n}_s^\tau = \frac{1}{N} \sum_{\mathbf{k}} \langle n_{ks}^\tau \rangle. \quad (23)$$

The total electron number per unit cell at τ valley is $\tilde{n}_\tau = \sum_s \tilde{n}_s^\tau$, lying in a domain of $[0,1]$. It is convenient for the following discussion to define the valley magnetization as

$$m_\tau = \tilde{n}_\uparrow^\tau - \tilde{n}_\downarrow^\tau, \quad m_{\bar{\tau}} = \tilde{n}_\uparrow^{\bar{\tau}} - \tilde{n}_\downarrow^{\bar{\tau}}, \quad (24)$$

which indicate the valley spin polarization. The total magnetization is then $m = m_\tau + m_{\bar{\tau}}$. When the ground state is spin

polarized, the total magnetization $m \neq 0$. In contrast, $m = 0$. In terms of \tilde{n}_τ and m_τ , the mean field is rewritten as

$$\mathbb{F}_{\tau s} = U(\tilde{n}_\tau + s m_\tau) - U'(\tilde{n}_{\bar{\tau}} + s m_{\bar{\tau}}). \quad (25)$$

The gap of the spin splitting of the conduction band is readily obtained,

$$\Delta_E^{\text{CT}}(\mathbf{k}) = E_{c\tau\uparrow}(\mathbf{k}) - E_{c\tau\downarrow}(\mathbf{k}) + \Delta_{\mathbb{F}}^\tau, \quad (26)$$

where $\Delta_{\mathbb{F}}^\tau = -2U m_\tau - 2U' m_{\bar{\tau}}$, which shows the influence of the e - e interaction on the spin splitting of the conduction band and indicates the renormalization of the conduction band minimum (CBM). The renormalized position of the CBM is self-consistently calculated. Parameters \tilde{n}_τ , m_τ , $\tilde{n}_{\bar{\tau}}$, and $m_{\bar{\tau}}$ constitute a four-dimensional parameter space. Any point in the space is denoted as a vector $(\tilde{n}_\tau, m_\tau, \tilde{n}_{\bar{\tau}}, m_{\bar{\tau}})$. At this stage, we have obtained all of the mean-field equations (MFEs), which are solved numerically and self-consistently. The procedure of the numerical calculation is as follows. First, we give a set of values for \tilde{n}_τ , m_τ , $\tilde{n}_{\bar{\tau}}$, and $m_{\bar{\tau}}$, which corresponds to a vector $\mathbf{P}_{\text{given}}$ in the parameter space. Then, the effective mean field $\mathbb{F}_{\tau s}$ is obtained by substituting \tilde{n}_τ , m_τ , $\tilde{n}_{\bar{\tau}}$, and $m_{\bar{\tau}}$ into Eq. (25). Utilizing Eq. (21), we get the energy spectrum. Finally, we calculate E_{free} by Eq. (22) and update \tilde{n}_τ , m_τ , $\tilde{n}_{\bar{\tau}}$, and $m_{\bar{\tau}}$ via Eqs. (C12) and (24). Note that parameter \tilde{n}_τ should be calculated via an integral over the momentum space and other parameters are not generated from integrals but from \tilde{n}_τ directly [see Eq. (24)]. \tilde{n}_τ is determined by the relative position of the energy with respect to the Fermi level (or the chemical potential) (see Appendix C). Hence, we neglect constant terms in the mean-field process which shift all energy bands equally and have no effect on the integral of \tilde{n}_τ and the self-consistent process. The updated $(\tilde{n}_\tau, m_\tau, \tilde{n}_{\bar{\tau}}, m_{\bar{\tau}})$ corresponds to a new point in the parameter space, denoted by a vector $\mathbf{P}_{\text{update}}$. We define the distance of the two points as the deviation:

$$\delta = |\mathbf{P}_{\text{given}} - \mathbf{P}_{\text{update}}|. \quad (27)$$

For a given point in the parameter space, if it is a solution of the set of MFEs, then δ is zero. We thus scan the entire parameter space and try to find the parameter vectors where δ converges to zero and we define these parameter vectors as the solutions.

III. NUMERICAL CALCULATIONS

It is found that the solution of MFEs is not unique (see Fig. 2) and the solutions are characterized by converged parameter vectors in the parameter space. In the numerical calculation, we grid the definitional domain of each parameter into \mathcal{N} subintervals, that is, the parameter space is gridded into \mathcal{N}^4 subspaces. As \mathcal{N} goes to infinite, the parameter space is ergodic exactly. In practice, we take a finite \mathcal{N} , and δ is kept at the order 10^{-6} . In this paper, we take $a = 3.193 \text{ \AA}$, $t = 1.1 \text{ eV}$, $\Delta = 1.66 \text{ eV}$, and $2\lambda = 0.15 \text{ eV}$, which are the fitting results to the *ab initio* calculation [13]. The intravalley Coulomb interaction U is usually unknown in TMDCs. According to the discussion of R. Roldán *et al.* [34], electronic states in the neighbor region of \mathbf{K} and \mathbf{K}' points are characterized by the $4d$ orbitals of Mo atoms. The order of

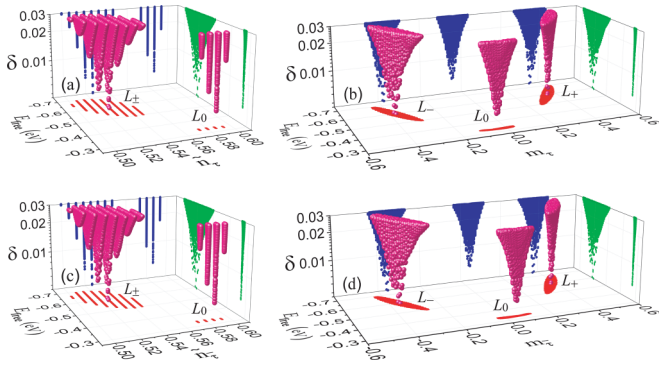


FIG. 2. Solutions of mean-field equations (MFEs). The parameter space is ergodic by gridding the space $150 \times 150 \times 150 \times 150$. We omit the points which have a derivation $\delta > 0.03$. The derivation δ of \tilde{n}_τ , m_τ , $\tilde{n}_{\bar{\tau}}$, and $m_{\bar{\tau}}$, are shown in (a)–(d). L_0 , L_+ , and L_- are the three solutions. The points in plane are projections of the red spheres. We take $U = 1.0$ eV, $U' = 0.4$ eV, and $\mu = 1.9$ eV

magnitude of U_{4d} is approximated by the ionization energy of Mo atoms. According to previous investigations of MoS₂ [34,35], one usually takes $U_{4d} \approx 2.0 \sim 4.0$ eV. We compare our definition of the interacting Hamiltonian with that of Rostami and Asgari [35], we find $U = U_{4d}/2$. Therefore, the intravalley Coulomb interaction is about $U \approx 1.0 \sim 2.0$ eV. Based on the above consideration, we take $U = 1.0$ eV and find the result is reasonable when U is combined with other parameter values.

Figure 2 shows the evolution of E_{free} and δ with \tilde{n}_τ , m_τ , $\tilde{n}_{\bar{\tau}}$, and $m_{\bar{\tau}}$ in (a)–(d), respectively ($\mathcal{N} = 150$). We obtain three solutions: one solution L_0 and two degenerated solutions L_\pm (with the same free energy). E_{free} is not the total free energy because the constant terms have been neglected in the calculation [see Eqs. (B1) and (B6)]. As for different mean-field solutions (L_0 , L_+ , and L_-), the values of the neglected constants are different. In Fig. 2, we plot the solutions L_0 , L_+ , and L_- on E_{free} for convenience without the meaning of comparison of free energy. L_\pm are solutions which haven't been obtained previously *due to ignoring the intervalley Coulomb interaction* [28,29]. In Figs. 2(a) and 2(c), $\tilde{n}_\tau(L_+)$ and $\tilde{n}_{\bar{\tau}}(L_+)$ are very close (the same to the solution of L_-). At the numerical precision $\delta \approx 10^{-6}$, we obtain the difference $\tilde{n}_\tau(L_+) - \tilde{n}_{\bar{\tau}}(L_+)$ is not zero but about an order of 10^{-4} , indicating a slight valley polarization. However, $\tilde{n}_\tau = \tilde{n}_{\bar{\tau}}$ for L_0 [see Figs. 2(a) and 2(c)]. As for L_0 , the states of τ and $\bar{\tau}$ valleys can be spin polarized but in opposite directions, which contributes a zero net magnetization [Figs. 2(b) and 2(d)]. In contrast, for solutions L_+ and L_- , spin polarization for both valleys can be induced as well but in the same direction, leading to a net magnetization for each solution. Because L_\pm are two degenerated solutions, the spin-polarized states (composed of two valleys) from L_+ and L_- are aligned opposite, giving rise to a zero net magnetization since the state of the entire system is randomly composed of the states of L_+ and L_- [25]. We further speculate that the states of L_\pm may manifest themselves by forming spin-polarized domains in real materials and, globally, there is no net magnetization without introducing an external magnetic field.

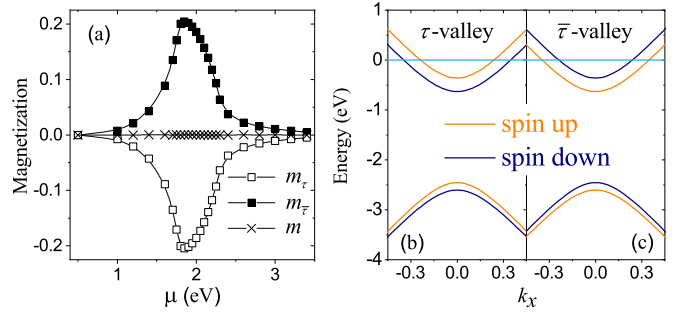


FIG. 3. (a) The dependence of m_τ , $m_{\bar{\tau}}$, and m on μ . $U = 1.0$ eV, $U' = 0$ eV. (b), (c) The energy spectrum $E_{\text{cvs}}(\mathbf{k})$ along k_x direction. $U = 1.0$ eV, $U' = 0$ eV, and $\mu = 1.7$ eV. The horizontal line shows the Fermi surface.

We first discuss the $U' = 0$ case, and the effective mean field becomes $\mathbb{F}_{\tau s} = \frac{2}{N} \sum_{\mathbf{k}} U \langle n_{\mathbf{k}s}^\tau \rangle$. We derive the solution L_0 that satisfies $\sum_{\mathbf{k}} \langle n_{\mathbf{k}\uparrow}^\tau \rangle = \sum_{\mathbf{k}} \langle n_{\mathbf{k}\downarrow}^\tau \rangle$ and $\sum_{\mathbf{k}} \langle n_{\mathbf{k}\downarrow}^\tau \rangle = \sum_{\mathbf{k}} \langle n_{\mathbf{k}\uparrow}^{\bar{\tau}} \rangle$. These indicate that the spin splitting of the conduction band at τ and $\bar{\tau}$ is inverted due to time-reversal symmetry (TRS) [see Figs. 3(b) and 3(c)] [13]. It can be seen from the energy gap in Eq. (26) at the minimum of the conduction band ($k = 0$), $\Delta_E^{\text{cr}}(0) = -2Um_\tau$. From Fig. 3(a), we find that $m_\tau = -m_{\bar{\tau}}$, and then $\Delta_E^{\text{cr}}(0)$ always takes the opposite values [see Figs. 3(b) and 3(c)]. We only derive the L_0 solution in this case, which means an unpolarized state in the absence of intervalley interaction.

In general, the intervalley $e-e$ interaction is comparable to the intravalley interaction even at high electron density, due to a small Bohr radius $a_B \sim 0.5$ nm [26]. In this case, all of \tilde{n}_τ , m_τ , $\tilde{n}_{\bar{\tau}}$, and $m_{\bar{\tau}}$ appear in the mean field $\mathbb{F}_{\tau s}$ [Eq. (25)], i.e., carriers in the two valleys interact with each other. Figure 4(a) shows the dependence of m on μ at various U' for the L_+ state. The main feature of the L_+ state is that there is a

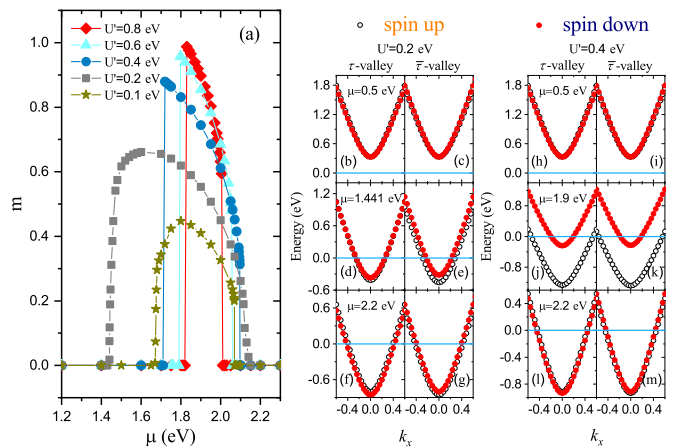


FIG. 4. (a) The dependence of m on μ at various U' . With the increase of μ , the solution of MFEs changes between L_0 and L_\pm . When the solutions are L_\pm , we merely chose L_+ and calculate m of L_+ , because L_+ and L_- are degenerate. (b)–(m) The spin splitting of the conduction band along the k_x direction. The horizontal lines represent the Fermi level. $U = 1.0$ eV.

region of gate voltage (characterized by chemical potential μ) in which a net magnetization is developed and characterized by a finite m . However, the global net magnetization is zero due to the superposition of the L_{\pm} states. We may call it a ferromagnetic (FM) state. Out of this region, $m = 0$ means a PM state. Therefore, there are two borders between the FM and PM states located at a lower and higher μ , which indicate a PM-FM phase transition and vice versa. However, three kinds of transitions are found. The first one is shown for $U' = 0.2$ eV, where m grows and disappears with μ continuously, indicating a second-order phase transition at two borders; the second one is shown for $U' = 0.4, 0.6,$ and 0.8 eV, where the PM-FM transitions are emergent discontinuously, which indicate a first-order phase transition consistent with the experimental observations [25]. The third one ($U' = 0.1$ eV) shows a second order and a first order at the lower and higher μ , respectively. As a theoretical investigation, we study the effects due to various parameters to cover most possibilities. The validity of the parameters should get support from experimental observations or other ways. Our results show that when $U' \geq 0.4$ eV, the phase transition is clearly of first order, which agrees with the experimental results [25]. This is also consistent with the previous prediction that the intervalley interaction is comparable with the intravalley interaction even at high electron density [26]. We therefore deduce that realistic intervalley Coulomb interaction should be in this range. The complicated transition behaviors exhibited in other parameter ranges might not be a reality. It is still lacking an intuitive picture for the appearance of such a complicated case.

To understand the existence of the FM state, we show band structures in Figs. 4(b)–4(m) and the relative positions of the Fermi level to CBM. The electron Coulomb interaction renormalizes the band structures (or the position of CBM). For different U' , the relative position of the Fermi level (or chemical potential) to the CBM is different. The PM states at small μ can be understood because the Fermi level does not pass through any bands [Figs. 4(b), 4(c), 4(h), and 4(i)]. For the PM states at large μ [Figs. 4(f), 4(g), 4(l), and 4(m)], the Fermi level deeply lies in all four bands where the e - e interaction may be weak due to a high electron density, and the spin splitting due to the e - e interaction is insignificant. In contrast to these two cases, Figs. 4(d), 4(e), 4(j), and 4(k) show the band structures for the FM states. It is noted that the spin splitting of bands is obviously observed and the Fermi level is not deeply lying in the conduction bands, but lies just around the bottom of some bands. This result matches our intuitive picture that the electron Coulomb interaction should be more important when the Fermi level is close to the CBM [24]. For Figs. 4(d) and 4(e), it seems a normal FM state in which the Fermi level is not far away from the bottom of the four bands. However, for Figs. 4(j) and 4(k), the Fermi level is deeply in the spin-up bands but shallowly lies in the spin-down bands. It might be this difference that leads to a different transition order between the PM and FM existing at lower and higher μ , respectively. It is obvious that the relative position of the Fermi level and the CBM is quite crucial for the existence of the FM states and this relative position is altered dramatically by including the electron Coulomb interaction and cannot be qualitatively predicted by thinking about the picture of the noninteraction case.

IV. DISCUSSIONS AND CONCLUSIONS

The complicated behaviors of the transition induced by μ may rest themselves into the fact that the energy bands are altered in the self-consistent MFEs. Comparable to the experiments, it seems that the first-order phase transitions at the two borders may be consistent with experimental observations [25]. If this is the case, we can deduce that the U' may be in the range of 0.4–0.8 eV. This energy scale may be converted to a length scale which corresponds to a Coulomb length for U' and a size of the so-called puddle in experiments, which is in 1–2 nm. This can be tested in experiments although this size is said to be small but not given in experiments. So far, we know that the polarized puddles resemble the domains in usual ferromagnets. In the zero- \mathbf{B} case, the polarizations of these puddles may be randomly distributed, giving rise to a zero net magnetization. We may speculate that the polarizations of puddles may be aligned into one direction when applying a nonzero \mathbf{B} , which brings us a net magnetization. This scenario is consistent with the experimental observation [24]. A further measurement on this size can clearly demonstrate our theory. We should emphasize that an FM state can be induced by tuning gate voltage due to finite U' . This reflects the important role of intervalley Coulomb interaction. The FM state can be derived only in the presence of intervalley Coulomb interaction. In the absence of the Coulomb interaction, Eq. (2) shows that the ground state is both valley and spin degenerate at $k = 0$. The conduction band at τ and $\bar{\tau}$ is inverted as the requirement of TRS. However, in the presence of the Coulomb interaction, it is found that the valley and spin degeneracy are lifted [Figs. 4(d), 4(e), 4(j), and 4(k)]. Note that the energy difference with the same spin index and various valley index in Figs. 4(j) and 4(k) is so small $|\mathbb{E}_{\tau\tau_s}(0) - \mathbb{E}_{\bar{\tau}\bar{\tau}_s}(0)| \approx 0.01$ eV that it is hard to be recognized. As shown in Figs. 4(d), 4(e), 4(j), and 4(k), intervalley Coulomb interaction combined with the suitable Fermi level induces the spin polarization of the ground state, which does not satisfy the requirement of TRS. Therefore, the TRS can be broken by the joint effects of intervalley Coulomb interaction and the Fermi level. A slight valley polarization (imbalanced of electrons distribution at τ and $\bar{\tau}$ valley) [14,36] can be induced by the e - e interaction at 10^{-3} order [see Figs. 4(j) and 4(k)]. When μ increases further, electron density is increased, e - e interaction is reduced, valley degeneracy and the TRS recovers again [see Figs. 4(l) and 4(m)].

ACKNOWLEDGMENTS

This work is supported in part by the National Key R&D Program of China (Grant No. 2018YFA0305800), the NSFC (Grants No. 11974348, No. 11674317, and No. 11834014). It is also supported by the Fundamental Research Funds for the Central Universities, and the Strategic Priority Research Program of CAS (Grants No. XDB28000000 and No. XDB33000000).

APPENDIX A: MODEL

1. Solve noninteracting Hamiltonian

According to the work reported by Xiao *et al.* [13], the effective Hamiltonian of ML-MoS₂ around Dirac cones without

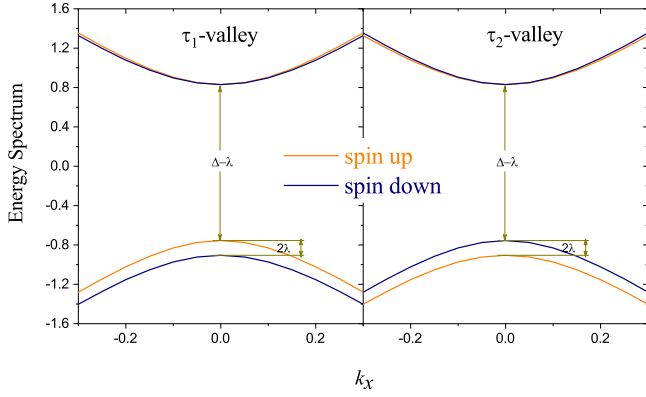


FIG. 5. Energy spectrum along k_x direction at τ_1 (left) and τ_2 (right) valleys. $a = 3.193 \text{ \AA}$, $t = 1.1 \text{ eV}$, $\Delta = 1.66 \text{ eV}$, and $2\lambda = 0.15 \text{ eV}$.

Coulomb interaction is

$$\hat{H}_0 = at(\tau k_x \sigma_x + k_y \sigma_y) + \frac{\Delta}{2} \sigma_z - \lambda \tau \frac{\sigma_z - 1}{2} \hat{s}_z, \quad (\text{A1})$$

where $\tau = \pm 1$ is the valley index. The spin splitting caused by spin-orbital coupling is 2λ . σ_α ($\alpha = x, y, z$) are the Pauli matrices. a is the lattice constant. t is the hopping integral. Δ is the energy gap between the conduction band and the valence band (when $\lambda = 0$). \hat{s}_z is the z component of the spin operator. For convenience, we choose a diamond BZ in the following calculation (see Fig. 6). We explicitly write

$$\hat{s}_z = \begin{pmatrix} s_{z1} & 0 \\ 0 & s_{z2} \end{pmatrix}, \quad \tau = \begin{pmatrix} \tau_1 & 0 \\ 0 & \tau_2 \end{pmatrix}, \quad (\text{A2})$$

where $s_{z1} = 1$ and $s_{z2} = -1$ represent spin up and spin down, respectively, $\tau_1 = 1$ and $\tau_2 = -1$ indicate the two valleys located at \mathbf{K} and \mathbf{K}' . We perform the direct product for the valley, spin, and band (conduction band and valence band) index freedom in the Hamiltonian. \hat{H}_0 is rewritten as

$$\hat{H}_0 = at(\tau \otimes k_x \sigma_x \otimes \mathbf{1} + \mathbf{1} \otimes k_y \sigma_y \otimes \mathbf{1}) + \mathbf{1} \otimes \frac{\Delta}{2} \sigma_z \otimes \mathbf{1} - \lambda \tau \otimes \frac{\sigma_z - 1}{2} \otimes \hat{s}_z, \quad (\text{A3})$$

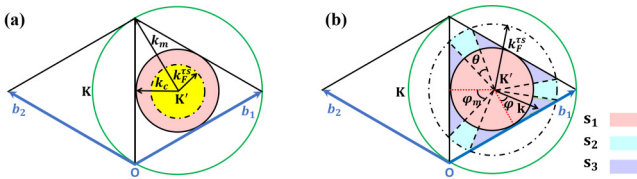


FIG. 6. The BZ of ML-MoS₂. \mathbf{b}_1 and \mathbf{b}_2 are the primitive vectors of the reciprocal lattice. \mathbf{K} and \mathbf{K}' marks two valleys. The black and green solid circles are the inscribed and circumscribed circles of the right half of BZ. The corresponding radius is k_c and k_m , as shown in (a). The inscribed circle is filled with rose color. k_F^{ts} is the Fermi radius. \mathbf{k} is any vector in BZ. (a) $0 \leq k_F^{ts} \leq k_c$. The region within the black dash-dot circle is occupied by the electrons and filled with yellow color. (b) $k_c < k_F^{ts} \leq k_m$. In this case, electrons occupy the colored region, which is composed of s_1 , s_2 , and s_3 . φ is the angle between \mathbf{k} and the red dot line. φ_m is the maximum of the angle.

where $\mathbf{1}$ is the identity matrix and \otimes denotes direct product. It is obvious that \hat{H}_0 is an 8×8 matrix. Substituting the Pauli matrix,

$$\sigma_x = \begin{pmatrix} 0 & 1 \\ 1 & 0 \end{pmatrix}, \quad \sigma_y = \begin{pmatrix} 0 & -i \\ i & 0 \end{pmatrix}, \quad \sigma_z = \begin{pmatrix} 1 & 0 \\ 0 & -1 \end{pmatrix} \quad (\text{A4})$$

into Eq. (A3), one obtains

$$\hat{H}_0 = \begin{pmatrix} \boldsymbol{\alpha} & \mathbf{0} \\ \mathbf{0} & \boldsymbol{\beta} \end{pmatrix}. \quad (\text{A5})$$

\hat{H}_0 is a block matrix, where $\mathbf{0}$, $\boldsymbol{\alpha}$, and $\boldsymbol{\beta}$ are 4×4 matrices. $\mathbf{0}$ is a zero matrix,

$$\boldsymbol{\alpha} = \begin{pmatrix} \frac{\Delta}{2} & 0 & \alpha_- & 0 \\ 0 & \frac{\Delta}{2} & 0 & \alpha_- \\ \alpha_+ & 0 & -\frac{\Delta}{2} + \lambda \tau_1 s_{z1} & 0 \\ 0 & \alpha_+ & 0 & -\frac{\Delta}{2} + \lambda \tau_1 s_{z2} \end{pmatrix}, \quad (\text{A6})$$

where $\alpha_{\pm} = at(\tau_1 k_x \pm ik_y)$, and

$$\boldsymbol{\beta} = \begin{pmatrix} \frac{\Delta}{2} & 0 & \beta_- & 0 \\ 0 & \frac{\Delta}{2} & 0 & \beta_- \\ \beta_+ & 0 & -\frac{\Delta}{2} + \lambda \tau_2 s_{z1} & 0 \\ 0 & \beta_+ & 0 & -\frac{\Delta}{2} + \lambda \tau_2 s_{z2} \end{pmatrix}, \quad (\text{A7})$$

where $\beta_{\pm} = at(\tau_2 k_x \pm ik_y)$. It is easy to diagonalize $\boldsymbol{\alpha}$ matrix. The energy eigenvalues for the τ_1 valley reads

$$E_{\tau_1 s_{z1}}^{(1)} = \frac{\lambda \tau_1 s_{z1}}{2} - \sqrt{(atk)^2 + \left(\frac{\Delta - \lambda \tau_1 s_{z1}}{2}\right)^2}, \quad (\text{A8})$$

$$E_{\tau_1 s_{z1}}^{(2)} = \frac{\lambda \tau_1 s_{z1}}{2} + \sqrt{(atk)^2 + \left(\frac{\Delta - \lambda \tau_1 s_{z1}}{2}\right)^2}, \quad (\text{A9})$$

$$E_{\tau_1 s_{z2}}^{(3)} = \frac{\lambda \tau_1 s_{z2}}{2} - \sqrt{(atk)^2 + \left(\frac{\Delta - \lambda \tau_1 s_{z2}}{2}\right)^2}, \quad (\text{A10})$$

$$E_{\tau_1 s_{z2}}^{(4)} = \frac{\lambda \tau_1 s_{z2}}{2} + \sqrt{(atk)^2 + \left(\frac{\Delta - \lambda \tau_1 s_{z2}}{2}\right)^2}. \quad (\text{A11})$$

The corresponding eigenvectors are

$$\mathbf{u}_{\tau_1 s_{z1}}^{(1)} = N_{\tau_1 s_{z1}}^{(1)} \begin{pmatrix} \frac{\Delta - 2E_{\tau_1 s_{z1}}^{(2)}}{2at(\tau_1 k_x + ik_y)}, 0, 1, 0 \end{pmatrix}^T, \quad (\text{A12})$$

$$\mathbf{u}_{\tau_1 s_{z1}}^{(2)} = N_{\tau_1 s_{z1}}^{(2)} \begin{pmatrix} \frac{\Delta - 2E_{\tau_1 s_{z1}}^{(1)}}{2at(\tau_1 k_x + ik_y)}, 0, 1, 0 \end{pmatrix}^T, \quad (\text{A13})$$

$$\mathbf{u}_{\tau_1 s_{z2}}^{(3)} = N_{\tau_1 s_{z2}}^{(3)} \begin{pmatrix} 0, \frac{\Delta - 2E_{\tau_1 s_{z2}}^{(4)}}{2at(\tau_1 k_x + ik_y)}, 0, 1 \end{pmatrix}^T, \quad (\text{A14})$$

$$\mathbf{u}_{\tau_1 s_{z2}}^{(4)} = N_{\tau_1 s_{z2}}^{(4)} \begin{pmatrix} 0, \frac{\Delta - 2E_{\tau_1 s_{z2}}^{(3)}}{2at(\tau_1 k_x + ik_y)}, 0, 1 \end{pmatrix}^T, \quad (\text{A15})$$

where the eigenvectors are normalized by

$$N_{\tau_1 s_{z1}}^{(1)} = \sqrt{\frac{4(atk)^2}{(\Delta - 2E_{\tau_1 s_{z1}}^{(2)})^2 + 4(atk)^2}}, \quad (\text{A16})$$

$$N_{\tau_1 s_{z1}}^{(2)} = \sqrt{\frac{4(atk)^2}{(\Delta - 2E_{\tau_1 s_{z1}}^{(1)})^2 + 4(atk)^2}}, \quad (\text{A17})$$

$$N_{\tau_1 s_2}^{(3)} = \sqrt{\frac{4(atk)^2}{(\Delta - 2E_{\tau_1 s_2}^{(4)})^2 + 4(atk)^2}}, \quad (\text{A18})$$

$$N_{\tau_1 s_2}^{(4)} = \sqrt{\frac{4(atk)^2}{(\Delta - 2E_{\tau_1 s_2}^{(3)})^2 + 4(atk)^2}}. \quad (\text{A19})$$

In the same way, we diagonalize the β matrix, obtaining the energy eigenvalues at τ_2 valley

$$E_{\tau_2 s_1}^{(5)} = \frac{\lambda \tau_2 s_{z_1}}{2} - \sqrt{(atk)^2 + \left(\frac{\Delta - \lambda \tau_2 s_{z_1}}{2}\right)^2}, \quad (\text{A20})$$

$$E_{\tau_2 s_1}^{(6)} = \frac{\lambda \tau_2 s_{z_1}}{2} + \sqrt{(atk)^2 + \left(\frac{\Delta - \lambda \tau_2 s_{z_1}}{2}\right)^2}, \quad (\text{A21})$$

$$E_{\tau_2 s_2}^{(7)} = \frac{\lambda \tau_2 s_{z_2}}{2} - \sqrt{(atk)^2 + \left(\frac{\Delta - \lambda \tau_2 s_{z_2}}{2}\right)^2}, \quad (\text{A22})$$

$$E_{\tau_2 s_2}^{(8)} = \frac{\lambda \tau_2 s_{z_2}}{2} + \sqrt{(atk)^2 + \left(\frac{\Delta - \lambda \tau_2 s_{z_2}}{2}\right)^2}. \quad (\text{A23})$$

The eigenvectors are

$$\mathbf{u}_{\tau_2 s_1}^{(5)} = N_{\tau_2 s_1}^{(5)} \left(\frac{\Delta - 2E_{\tau_2 s_1}^{(6)}}{2at(\tau_2 k_x + ik_y)}, 0, 1, 0 \right)^T, \quad (\text{A24})$$

$$\mathbf{u}_{\tau_2 s_1}^{(6)} = N_{\tau_2 s_1}^{(6)} \left(\frac{\Delta - 2E_{\tau_2 s_1}^{(5)}}{2at(\tau_2 k_x + ik_y)}, 0, 1, 0 \right)^T, \quad (\text{A25})$$

$$\mathbf{u}_{\tau_2 s_2}^{(7)} = N_{\tau_2 s_2}^{(7)} \left(0, \frac{\Delta - 2E_{\tau_2 s_2}^{(8)}}{2at(\tau_2 k_x + ik_y)}, 0, 1 \right)^T, \quad (\text{A26})$$

$$\mathbf{u}_{\tau_2 s_2}^{(8)} = N_{\tau_2 s_2}^{(8)} \left(0, \frac{\Delta - 2E_{\tau_2 s_2}^{(7)}}{2at(\tau_2 k_x + ik_y)}, 0, 1 \right)^T, \quad (\text{A27})$$

where

$$N_{\tau_2 s_1}^{(5)} = \sqrt{\frac{4(atk)^2}{(\Delta - 2E_{\tau_2 s_1}^{(6)})^2 + 4(atk)^2}}, \quad (\text{A28})$$

$$N_{\tau_2 s_1}^{(6)} = \sqrt{\frac{4(atk)^2}{(\Delta - 2E_{\tau_2 s_1}^{(5)})^2 + 4(atk)^2}}, \quad (\text{A29})$$

$$N_{\tau_2 s_2}^{(7)} = \sqrt{\frac{4(atk)^2}{(\Delta - 2E_{\tau_2 s_2}^{(8)})^2 + 4(atk)^2}}, \quad (\text{A30})$$

$$N_{\tau_2 s_2}^{(8)} = \sqrt{\frac{4(atk)^2}{(\Delta - 2E_{\tau_2 s_2}^{(7)})^2 + 4(atk)^2}}. \quad (\text{A31})$$

Energy eigenvalues are written compactly as [32]

$$E_{n\tau s} = \frac{1}{2} \lambda \tau s \pm \sqrt{(atk)^2 + \left(\frac{\Delta - \lambda \tau s}{2}\right)^2}, \quad (\text{A32})$$

where the spin index $s = s_{z_1}$ or s_{z_2} . $E_{n\tau s}$ is shown in Fig. 5. The up plus sign denotes the conduction band (c). The bottom minus sign denotes the valence band (v). n is the band index (conduction band $n = c$, valence band $n = v$). k is the module of the wave vector, $k = \sqrt{k_x^2 + k_y^2}$. The valley index $\tau = \tau_1$ or τ_2 . The corresponding eigenstate is a superposition state of the bases [13] with the coefficients defined by the eigenvectors, which is denoted as $|n\tau ks\rangle = \psi_{n\tau s}(\mathbf{k}, \mathbf{r})$.

2. Coulomb interaction

Electron-electron ($e-e$) interactions have significant effects on the physical properties of monolayer materials [18]. As early as 1979, Keldysh investigated Coulomb interaction in thin semiconductor and semimetal films, and gave an effective Coulomb interaction, which is expressed by the Neumann and Struve functions [37]. In this paper, we focused on a qualitative discussion. Therefore, we take the usual bare Coulomb interaction instead of the complicated potential given by Keldysh. The bare Coulomb interaction is

$$V(\mathbf{r}_1 - \mathbf{r}_2) = \frac{e^2}{4\pi\epsilon_0} \frac{1}{|\mathbf{r}_1 - \mathbf{r}_2|}, \quad (\text{A33})$$

where e is the elementary charge, ϵ_0 is the vacuum permittivity. It is obvious that in terms of field operators, the Coulomb interaction is written as [33]

$$\hat{V}(\mathbf{r}_1 - \mathbf{r}_2) = \frac{1}{2} \sum_{s_1 s_2} \iint d\mathbf{r}_1 d\mathbf{r}_2 V(\mathbf{r}_1 - \mathbf{r}_2) \psi_{s_1}^\dagger(\mathbf{r}_1) \psi_{s_2}^\dagger(\mathbf{r}_2) \psi_{s_2}(\mathbf{r}_2) \psi_{s_1}(\mathbf{r}_1). \quad (\text{A34})$$

We take the transformation

$$\psi_s^\dagger(\mathbf{r}) = \frac{1}{\sqrt{N}} \sum_{n\tau k} \psi_{n\tau s}^*(\mathbf{k}, \mathbf{r}) a_{ks}^{n\tau\dagger}, \quad (\text{A35})$$

$$\psi_s(\mathbf{r}) = \frac{1}{\sqrt{N}} \sum_{n\tau k} \psi_{n\tau s}(\mathbf{k}, \mathbf{r}) a_{ks}^{n\tau}. \quad (\text{A36})$$

It is secondly quantized in the $|n\tau ks\rangle$ representation [33]

$$\hat{V} = \frac{1}{N} \sum_{s_1 s_2} \sum_{\mathbf{k}_1 \mathbf{k}_2} \sum_{\mathbf{k}_3 \mathbf{k}_4} \sum_{n_1 n_2} \sum_{n_3 n_4} \times \sum_{\tau_1 \tau_2} \sum_{\tau_3 \tau_4} V_{\text{int}} a_{\mathbf{k}_1 s_1}^{n_1 \tau_1 \dagger} a_{\mathbf{k}_2 s_2}^{n_2 \tau_2 \dagger} a_{\mathbf{k}_3 s_2}^{n_3 \tau_3} a_{\mathbf{k}_4 s_1}^{n_4 \tau_4}, \quad (\text{A37})$$

where V_{int} denotes the strength of the $e-e$ interaction and N is the number of the unit cell. $a_{ks}^{n\tau\dagger}$ ($a_{ks}^{n\tau}$) is the creation (annihilation) operator at $|n\tau ks\rangle$ state. Because the valence band is fully filled, we only consider the $e-e$ interaction in the conduction band, i.e., $n = c$. In the following derivation, the superscript c is omitted. We take the summation of τ_2 , τ_3 , and τ_4 in Eq. (A37), obtaining

$$\hat{V} = \frac{1}{N} \sum_{\tau_1 s_2} \sum_{\mathbf{k}_1 \mathbf{k}_2 \mathbf{k}_3 \mathbf{k}_4} \sum_{i=1}^8 V_{\text{int}}^{(i)} T_i, \quad (\text{A38})$$

where T_i reads

$$T_1 = a_{\mathbf{k}_1 s_1}^{\tau_1 \dagger} a_{\mathbf{k}_2 s_2}^{\tau_1 \dagger} a_{\mathbf{k}_3 s_2}^{\tau_1} a_{\mathbf{k}_4 s_1}^{\tau_1}, \quad (\text{A39})$$

$$T_2 = a_{\mathbf{k}_1 s_1}^{\tau_1 \dagger} a_{\mathbf{k}_2 s_2}^{\tau_1 \dagger} a_{\mathbf{k}_3 s_2}^{\tau_1} a_{\mathbf{k}_4 s_1}^{\bar{\tau}_1}, \quad (\text{A40})$$

$$T_3 = a_{\mathbf{k}_1 s_1}^{\tau_1 \dagger} a_{\mathbf{k}_2 s_2}^{\tau_1 \dagger} a_{\mathbf{k}_3 s_2}^{\bar{\tau}_1} a_{\mathbf{k}_4 s_1}^{\tau_1}, \quad (\text{A41})$$

$$T_4 = a_{\mathbf{k}_1 s_1}^{\tau_1 \dagger} a_{\mathbf{k}_2 s_2}^{\tau_1 \dagger} a_{\mathbf{k}_3 s_2}^{\bar{\tau}_1} a_{\mathbf{k}_4 s_1}^{\bar{\tau}_1}, \quad (\text{A42})$$

$$T_5 = a_{\mathbf{k}_1 s_1}^{\tau_1 \dagger} a_{\mathbf{k}_2 s_2}^{\bar{\tau}_1 \dagger} a_{\mathbf{k}_3 s_2}^{\tau_1} a_{\mathbf{k}_4 s_1}^{\tau_1}, \quad (\text{A43})$$

$$T_6 = a_{\mathbf{k}_1 s_1}^{\tau_1 \dagger} a_{\mathbf{k}_2 s_2}^{\bar{\tau}_1 \dagger} a_{\mathbf{k}_3 s_2}^{\tau_1} a_{\mathbf{k}_4 s_1}^{\bar{\tau}_1}, \quad (\text{A44})$$

$$T_7 = a_{k_1 s_1}^{\tau\dagger} a_{k_2 s_2}^{\bar{\tau}\dagger} a_{k_3 s_2}^{\bar{\tau}} a_{k_4 s_1}^{\tau}, \quad (\text{A45})$$

$$T_8 = a_{k_1 s_1}^{\tau\dagger} a_{k_2 s_2}^{\bar{\tau}\dagger} a_{k_3 s_2}^{\bar{\tau}} a_{k_4 s_1}^{\bar{\tau}}. \quad (\text{A46})$$

It is obvious that T_1 gives the intravalley e - e interaction. T_2 , T_3 , T_4 , T_5 , and T_8 describe the electron transformation from one valley to the other, which is not considered in this paper. T_7 shows the intravalley transformation of electrons without exchanges of spin, which is also neglected. T_6 gives the intervalley spin exchange coupling. The interaction-induced magnetic order transition of the ground state is attributed to this term, which is taken into consideration carefully. The strength of the interaction corresponding to T_i reads

$$V_{\text{int}}^{(1)} = \frac{1}{2N} \langle \tau k_1, \tau k_2 | V(\mathbf{r}_1 - \mathbf{r}_2) | \tau k_4, \tau k_3 \rangle, \quad (\text{A47})$$

$$V_{\text{int}}^{(2)} = \frac{1}{2N} \langle \tau k_1, \tau k_2 | V(\mathbf{r}_1 - \mathbf{r}_2) | \bar{\tau} k_4, \tau k_3 \rangle, \quad (\text{A48})$$

$$V_{\text{int}}^{(3)} = \frac{1}{2N} \langle \tau k_1, \tau k_2 | V(\mathbf{r}_1 - \mathbf{r}_2) | \tau k_4, \bar{\tau} k_3 \rangle, \quad (\text{A49})$$

$$V_{\text{int}}^{(4)} = \frac{1}{2N} \langle \tau k_1, \tau k_2 | V(\mathbf{r}_1 - \mathbf{r}_2) | \bar{\tau} k_4, \bar{\tau} k_3 \rangle, \quad (\text{A50})$$

$$V_{\text{int}}^{(5)} = \frac{1}{2N} \langle \tau k_1, \bar{\tau} k_2 | V(\mathbf{r}_1 - \mathbf{r}_2) | \tau k_4, \tau k_3 \rangle, \quad (\text{A51})$$

$$V_{\text{int}}^{(6)} = \frac{1}{2N} \langle \tau k_1, \bar{\tau} k_2 | V(\mathbf{r}_1 - \mathbf{r}_2) | \bar{\tau} k_4, \tau k_3 \rangle, \quad (\text{A52})$$

$$V_{\text{int}}^{(7)} = \frac{1}{2N} \langle \tau k_1, \bar{\tau} k_2 | V(\mathbf{r}_1 - \mathbf{r}_2) | \tau k_4, \bar{\tau} k_3 \rangle, \quad (\text{A53})$$

$$V_{\text{int}}^{(8)} = \frac{1}{2N} \langle \tau k_1, \bar{\tau} k_2 | V(\mathbf{r}_1 - \mathbf{r}_2) | \bar{\tau} k_4, \bar{\tau} k_3 \rangle. \quad (\text{A54})$$

$\bar{\tau}$ (\bar{s}) represents the opposite valley (spin) of τ (s). \mathbf{k} ($\bar{\mathbf{k}}$) indicates the relative wave vector with respect to the minimum of τ ($\bar{\tau}$) valley. As for T_1 , we take $s_2 = \bar{s}_1$. Due to the Pauli exclusion principle, electrons with the opposite spin are apt to be spatially closer than those with the same spin. Therefore, the contribution of the term $s_2 = s_1$ is omitted. The momentum conservation is employed. In the T_1 term, we take $\mathbf{k}_4 = \mathbf{k}_1$ and $\mathbf{k}_3 = \mathbf{k}_2$. As for T_6 , we are focused on the spin exchange and neglect the momentum scattering in the process. Therefore, we take $\mathbf{k}_3 = \mathbf{k}_1$ and $\mathbf{k}_4 = \mathbf{k}_2$. It is convenient to define $U = V_{\text{int}}^{(1)}$ and $U' = V_{\text{int}}^{(6)}$. The intravalley and intervalley e - e interaction are then written as

$$\hat{V}_{\text{intra}} = \frac{1}{N} \sum_{\tau s} \sum_{k_1 k_2} U a_{k_1 s}^{\tau\dagger} a_{k_2 \bar{s}}^{\tau\dagger} a_{k_2 s}^{\tau} a_{k_1 \bar{s}}^{\tau}, \quad (\text{A55})$$

$$\hat{V}_{\text{inter}} = \frac{1}{N} \sum_{\tau s_1 s_2} \sum_{k_1 k_2} U' a_{k_1 s_1}^{\tau\dagger} a_{k_2 s_2}^{\bar{\tau}\dagger} a_{k_1 s_2}^{\tau} a_{k_2 s_1}^{\bar{\tau}}. \quad (\text{A56})$$

Therefore, the total Hamiltonian is obtained,

$$\hat{H} = \hat{H}_0 + \hat{V}_{\text{intra}} + \hat{V}_{\text{inter}}, \quad (\text{A57})$$

which includes the intravalley and intervalley interaction. In the following, \hat{H} is solved at the mean-field level.

APPENDIX B: MEAN-FIELD APPROXIMATION

As for \hat{V}_{intra} , we take the MFA directly:

$$\begin{aligned} \hat{V}_{\text{intra}}^{\text{MF}} &= \frac{1}{N} \sum_{\tau s} \sum_{k_1 k_2} U \left(\langle a_{k_1 s}^{\tau\dagger} a_{k_1 s}^{\tau} \rangle a_{k_2 \bar{s}}^{\tau\dagger} a_{k_2 \bar{s}}^{\tau} \right. \\ &\quad \left. + a_{k_1 s}^{\tau\dagger} a_{k_1 s}^{\tau} \langle a_{k_2 \bar{s}}^{\tau\dagger} a_{k_2 \bar{s}}^{\tau} \rangle - \langle a_{k_1 s}^{\tau\dagger} a_{k_1 s}^{\tau} \rangle \langle a_{k_2 \bar{s}}^{\tau\dagger} a_{k_2 \bar{s}}^{\tau} \rangle \right). \end{aligned} \quad (\text{B1})$$

In the MFA, we neglect the second-order quantum fluctuations. The third term in the above equation is omitted because it is a constant, which cannot effect the following qualitative discussion of the result. The MFA of \hat{V}_{intra} reads

$$\begin{aligned} \hat{V}_{\text{intra}}^{\text{MF}} &\approx \frac{1}{N} \sum_{\tau s} \sum_{k_1 k_2} U \left(\langle n_{k_1 s}^{\tau} \rangle n_{k_2 \bar{s}}^{\tau} + n_{k_1 s}^{\tau} \langle n_{k_2 \bar{s}}^{\tau} \rangle \right) \\ &\approx \frac{2}{N} \sum_{\tau s} \sum_{k_1 k_2} U \langle n_{k_2 \bar{s}}^{\tau} \rangle n_{k_1 s}^{\tau} \\ &\approx \sum_{\tau k s} \mathbb{U}_{\tau s} a_{k s}^{\tau\dagger} a_{k s}^{\tau}, \end{aligned} \quad (\text{B2})$$

where

$$\mathbb{U}_{\tau s} = \frac{2}{N} \sum_k U \langle n_{k \bar{s}}^{\tau} \rangle. \quad (\text{B3})$$

$n_{k s}^{\tau} = a_{k s}^{\tau\dagger} a_{k s}^{\tau}$ is the particle number operator. Here, we merely consider the zero temperature case. So, $\langle \dots \rangle$ is the ground-state average. As for \hat{V}_{inter} , we rewrite it in terms of the spin operators to extract the intervalley spin exchange interaction:

$$\hat{V}_{\text{inter}} = -\frac{1}{N} \sum_{k_1 k_2} U' \left(n_{k_1}^{\tau} n_{k_2}^{\bar{\tau}} + 4 \mathbf{S}_{\tau k_1} \cdot \mathbf{S}_{\bar{\tau} k_2} \right). \quad (\text{B4})$$

The spin coupling term reads

$$\mathbf{S}_{\tau k_1} \cdot \mathbf{S}_{\bar{\tau} k_2} = S_{\tau k_1}^z S_{\bar{\tau} k_2}^z + \frac{1}{2} \left(S_{\tau k_1}^+ S_{\bar{\tau} k_2}^- + S_{\tau k_1}^- S_{\bar{\tau} k_2}^+ \right), \quad (\text{B5})$$

where $S_{\tau k}^z = \frac{1}{2} (n_{k\uparrow}^{\tau} - n_{k\downarrow}^{\tau})$, $S_{\tau k}^+ = a_{k\uparrow}^{\tau\dagger} a_{k\downarrow}^{\tau}$, and $S_{\tau k}^- = a_{k\downarrow}^{\tau\dagger} a_{k\uparrow}^{\tau}$. It is obvious that the intervalley spin coupling is extracted. We chose the direction of \mathbf{S} as the z axis and apply the MFA to Eq. (B4), obtaining

$$\begin{aligned} \hat{V}_{\text{inter}}^{\text{MF}} &= -\frac{1}{N} \sum_{k_1 k_2} U' \left(\langle n_{k_1}^{\tau} \rangle \langle n_{k_2}^{\bar{\tau}} \rangle + n_{k_1}^{\tau} \langle n_{k_2}^{\bar{\tau}} \rangle - \langle n_{k_1}^{\tau} \rangle \langle n_{k_2}^{\bar{\tau}} \rangle \right) \\ &\quad + 4 \langle S_{\tau k_1}^z \rangle S_{\bar{\tau} k_2}^z + 4 S_{\tau k_1}^z \langle S_{\bar{\tau} k_2}^z \rangle - 4 \langle S_{\tau k_1}^z \rangle \langle S_{\bar{\tau} k_2}^z \rangle \\ &\approx - \sum_{\tau k} \left(\mathbb{U}'_{\tau} n_{k}^{\tau} + \mathbb{M}_{\tau} S_{\tau k}^z \right) \\ &\approx - \sum_{\tau k s} \left(\mathbb{U}'_{\tau} + \frac{1}{2} s \mathbb{M}_{\tau} \right) n_{k s}^{\tau} \\ &\approx - \sum_{\tau k s} \mathbb{X}_{\tau s} a_{k s}^{\tau\dagger} a_{k s}^{\tau} \end{aligned} \quad (\text{B6})$$

where

$$\mathbb{U}'_{\tau} = \frac{1}{N} \sum_{\mathbf{k}} U' \langle n_{\mathbf{k}}^{\tau} \rangle, \quad (\text{B7})$$

$$\mathbb{M}_{\tau} = \frac{4}{N} \sum_{\mathbf{k}} U' \langle S_{\tau\mathbf{k}}^z \rangle, \quad (\text{B8})$$

$$\mathbb{X}_{\tau s} = \mathbb{U}'_{\tau} + \frac{1}{2} s \mathbb{M}_{\tau}. \quad (\text{B9})$$

Therefore, the MFA of the interaction operator $\hat{\mathbb{V}}$ is

$$\begin{aligned} \hat{\mathbb{V}}_{\text{MF}} &= \hat{\mathbb{V}}_{\text{intra}}^{\text{MF}} + \hat{\mathbb{V}}_{\text{inter}}^{\text{MF}} \\ &= \sum_{ks} (\mathbb{F}_{\tau s} a_{ks}^{\tau\dagger} a_{ks}^{\tau} + \mathbb{F}_{\tau s} a_{\bar{k}s}^{\tau\dagger} a_{\bar{k}s}^{\tau}), \end{aligned} \quad (\text{B10})$$

where the effective mean field is

$$\mathbb{F}_{\tau s} = \mathbb{U}_{\tau s} - \mathbb{X}_{\tau s}. \quad (\text{B11})$$

At the mean-field level, the total Hamiltonian reads

$$\mathbb{H}_{\text{total}}^{\text{MF}} = \sum_{ks} (\mathbb{E}_{c\tau s}(\mathbf{k}) a_{ks}^{\tau\dagger} a_{ks}^{\tau} + \mathbb{E}_{c\bar{\tau}s}(\bar{\mathbf{k}}) a_{\bar{k}s}^{\tau\dagger} a_{\bar{k}s}^{\tau}), \quad (\text{B12})$$

where the energy spectrum is

$$\mathbb{E}_{c\tau s}(\mathbf{k}) = E_{c\tau s}(\mathbf{k}) + \mathbb{F}_{\tau s} - \mu. \quad (\text{B13})$$

It is obvious that the effective mean field $\mathbb{F}_{\tau s}$ is obtained upon the calculation of $\langle n_{ks}^{\tau} \rangle$. It is convenient to define

$$\tilde{n}_s^{\tau} = \frac{1}{N} \sum_{\mathbf{k}} \langle n_{\mathbf{k}s}^{\tau} \rangle, \quad (\text{B14})$$

which indicates the ratio of the occupation at τ valley. Equations (A32), (B3), (B7)–(B9), and (B11)–(B14) constitute a set of mean-field self-consistent equations.

APPENDIX C: CALCULATIONS ON \tilde{n}_s^{τ} AND E_{free}

In this Appendix, we calculate \tilde{n}_s^{τ} and E_{free} . The BZ of ML-MoS₂ is shown in Fig. 6. \mathbf{b}_1 and \mathbf{b}_2 are the two primitive vectors of the BZ:

$$\mathbf{b}_1 = \left(\frac{2\pi}{\sqrt{3}a}, \frac{2\pi}{3a} \right), \quad \mathbf{b}_2 = \left(-\frac{2\pi}{\sqrt{3}a}, \frac{2\pi}{3a} \right). \quad (\text{C1})$$

It is easy to obtain the area of BZ, $S_{\text{BZ}} = 8\sqrt{3}\pi^2/9a^2$. For simplicity and compactness of the formula, we define $\mathbb{A}_{\tau s} = \lambda\tau s/2 - \mu + \mathbb{F}_{\tau s}$ and $\mathbb{B}_{\tau s} = (\Delta - \lambda\tau s)/2$. The energy spectrum is rewritten as

$$\mathbb{E}_{c\tau s}(\mathbf{k}) = \mathbb{A}_{\tau s} \pm \sqrt{(atk)^2 + \mathbb{B}_{\tau s}^2}. \quad (\text{C2})$$

If $\mathbb{A}_{\tau s} \leq 0$ and $|\mathbb{A}_{\tau s}| \geq |\mathbb{B}_{\tau s}|$, we are able to solve $\mathbb{E}_{c\tau s}(k) = 0$ and obtain the Fermi radius

$$k_F^{\tau s} = \frac{1}{at} \sqrt{\mathbb{A}_{\tau s}^2 - \mathbb{B}_{\tau s}^2}. \quad (\text{C3})$$

As shown in Fig. 6(a), if $0 \leq k_F^{\tau s} \leq k_c$, electrons occupy the yellow region of the BZ. If $k_c < k_F^{\tau s} \leq k_m$, electrons occupy the colored region as shown in Fig. 6(b). $k_c = 2\sqrt{3}\pi/9a$ and $k_m = 2k_c$ are the radius of the inscribed and circumscribed circles of the right half of the BZ. Instead of the summation

of the discrete values in Eq. (B14), we take the value of k continuously. The definition of \tilde{n}_s^{τ} is rewritten equivalently as

$$\tilde{n}_s^{\tau} = \frac{S_{\text{occ}}^{\tau s}}{S_{\text{BZ}}}, \quad (\text{C4})$$

where $S_{\text{occ}}^{\tau s}$ is the area of the region which is occupied by the electron. When $0 \leq k_F^{\tau s} \leq k_c$,

$$S_{\text{occ}}^{\tau s} = \pi (k_F^{\tau s})^2. \quad (\text{C5})$$

Substituting into Eq.(C4), we obtain

$$\tilde{n}_s^{\tau} = \frac{3\sqrt{3}a^2 (k_F^{\tau s})^2}{8\pi}. \quad (\text{C6})$$

When $k_c < k_F^{\tau s} \leq k_m$, $S_{\text{occ}}^{\tau s}$ is divided into two parts: three triangle areas and three sectorial areas [see Fig. 6(b), regions divided by dash lines]:

$$S_{\text{occ}}^{\tau s} = S_{\text{tri}}^{\tau s} + S_{\text{sec}}^{\tau s}. \quad (\text{C7})$$

As for $S_{\text{tri}}^{\tau s}$, we have

$$S_{\text{tri}}^{\tau s} = 3k_c \sqrt{(k_F^{\tau s})^2 - k_c^2}. \quad (\text{C8})$$

The sectorial area is

$$S_{\text{sec}}^{\tau s} = \frac{3}{2} (k_F^{\tau s})^2 \theta, \quad (\text{C9})$$

where θ is the angle of the sector. Therefore,

$$S_{\text{occ}}^{\tau s} = 3k_c \sqrt{(k_F^{\tau s})^2 - k_c^2} + \frac{3}{2} (k_F^{\tau s})^2 \theta. \quad (\text{C10})$$

Substituting into Eq. (C4), we have

$$\tilde{n}_s^{\tau} = \frac{3a}{4\pi} \sqrt{(k_F^{\tau s})^2 - k_c^2} + \frac{\sqrt{3}}{12} \left(\frac{k_F^{\tau s}}{k_c} \right)^2 \theta. \quad (\text{C11})$$

When $k_F^{\tau s} > k_m$, $S_{\text{occ}}^{\tau s}$ is half of S_{BZ} . Therefore, $\tilde{n}_s^{\tau} = 1/2$. Conclusively,

$$\tilde{n}_s^{\tau} = \begin{cases} \frac{3\sqrt{3}a^2 (k_F^{\tau s})^2}{8\pi} & 0 \leq k_F^{\tau s} \leq k_c \\ \frac{3a}{4\pi} \sqrt{(k_F^{\tau s})^2 - k_c^2} + \frac{\sqrt{3}}{12} \left(\frac{k_F^{\tau s}}{k_c} \right)^2 \theta & k_c < k_F^{\tau s} \leq k_m \\ \frac{1}{2} & k_m < k_F^{\tau s}, \end{cases} \quad (\text{C12})$$

where

$$\theta = 2\arcsin \left(\frac{\pi}{3ak_F^{\tau s}} - \frac{1}{2k_F^{\tau s}} \sqrt{(k_F^{\tau s})^2 - k_c^2} \right). \quad (\text{C13})$$

As for the electron which fills the conduction band, its contribution to the free energy is defined by the integration

$$E_{\text{free}}^{\tau s} = \int_{S_{\text{occ}}^{\tau s}} d\mathbf{k} \left(\mathbb{A}_{\tau s} + \sqrt{(atk)^2 + \mathbb{B}_{\tau s}^2} \right). \quad (\text{C14})$$

Hence, the total free energy reads

$$E_{\text{free}} = \sum_{\tau s} E_{\text{free}}^{\tau s}. \quad (\text{C15})$$

In Eq. (C14), we neglect the wave vector density. When $0 \leq k_F^{\tau s} \leq k_c$, the region occupied by the electrons in BZ is a circular region. $E_{\text{free}}^{\tau s}$ is calculated directly.

$$\begin{aligned} E_{\text{free}}^{\tau s} &= - \int_{\mathbb{E}_{\text{cts}}(0)}^{\mathbb{E}_{\text{cts}}(k_F^{\tau s})} \pi k^2 d\mathbb{E} \\ &= - \int_{\mathbb{E}_{\text{cts}}(0)}^{\mathbb{E}_{\text{cts}}(k_F^{\tau s})} \frac{\pi}{(at)^2} [(\mathbb{E} - \mathbb{A}_{\tau s})^2 - \mathbb{B}_{\tau s}^2] d\mathbb{E} \\ &= \frac{\pi}{3(at)^2} (\mathbb{A}_{\tau s}^3 - 2\mathbb{B}_{\tau s}^3 - 3\mathbb{B}_{\tau s}^2 \mathbb{A}_{\tau s}). \end{aligned} \quad (\text{C16})$$

In the above derivation, we use $\mathbb{E}(k_F^{\tau s}) = 0$ and $\mathbb{E}(0) = \mathbb{A}_{\tau s} + \mathbb{B}_{\tau s}$. As for the case $k_c < k_F^{\tau s} \leq k_m$, $E_{\text{free}}^{\tau s}$ is composed of three parts, which are corresponding to the integration over the region s_1 , s_2 , and s_3 as shown in Fig. 6(b),

$$E_{\text{free}}^{\tau s} = E_1^{\tau s} + E_2^{\tau s} + E_3^{\tau s}. \quad (\text{C17})$$

We calculate the integration individually.

(1) The integration in region s_1 is

$$\begin{aligned} E_1^{\tau s} &= - \int_{\mathbb{E}_{\text{cts}}(0)}^{\mathbb{E}_{\text{cts}}(k_c)} \pi k^2 d\mathbb{E} - \int_{\mathbb{E}_{\text{cts}}(k_c)}^{\mathbb{E}_{\text{cts}}(k_F^{\tau s})} \pi k_c^2 d\mathbb{E} \\ &= - \int_{\mathbb{E}_{\text{cts}}(0)}^{\mathbb{E}_{\text{cts}}(k_c)} \frac{\pi}{(at)^2} [(\mathbb{E} - \mathbb{A}_{\tau s})^2 - \mathbb{B}_{\tau s}^2] d\mathbb{E} \\ &\quad + \pi k_c^2 \mathbb{E}_{\text{cts}}(k_c) \\ &= \frac{\pi}{3(at)^2} (3\mathbb{B}_{\tau s}^2 \mathbb{C}_{\tau s} - \mathbb{C}_{\tau s}^3 - 2\mathbb{B}_{\tau s}^3) \\ &\quad + \pi k_c^2 \mathbb{E}_{\text{cts}}(k_c), \end{aligned} \quad (\text{C18})$$

where

$$\mathbb{C}_{\tau s} = \sqrt{(atk_c)^2 + \mathbb{B}_{\tau s}^2}. \quad (\text{C19})$$

(2) The integration in region s_2 is

$$\begin{aligned} E_2^{\tau s} &= \frac{3\theta}{2\pi} \left(- \int_{\mathbb{E}_{\text{cts}}(0)}^{\mathbb{E}_{\text{cts}}(k_F^{\tau s})} \pi k^2 d\mathbb{E} - E_1^{\tau s} \right) \\ &= \frac{\theta}{2(at)^2} (\mathbb{A}_{\tau s}^3 - 2\mathbb{B}_{\tau s}^3 - 3\mathbb{B}_{\tau s}^2 \mathbb{A}_{\tau s}) - \frac{3\theta}{2\pi} E_1^{\tau s}. \end{aligned} \quad (\text{C20})$$

(3) The integration in region s_3 is complicated. We have

$$\begin{aligned} E_3^{\tau s} &= 6 \int_{s_3} \mathbb{A}_{\tau s} + \sqrt{(atk)^2 + \mathbb{B}_{\tau s}^2} dk_x dk_y \\ &= 6 \int_0^{\varphi_m} d\varphi \int_{k_c}^{k_c/\cos(\varphi)} k \left(\mathbb{A}_{\tau s} + \sqrt{(atk)^2 + \mathbb{B}_{\tau s}^2} \right) dk \\ &= 6 \int_0^{\varphi_m} d\varphi \left\{ \frac{1}{2} \mathbb{A}_{\tau s} k_c^2 \left(\frac{1}{\cos^2(\varphi)} - 1 \right) \right. \\ &\quad \left. + \frac{1}{3(at)^2} \left[\left(\frac{atk_c}{\cos(\varphi)} \right)^2 + \mathbb{B}_{\tau s}^2 \right]^{\frac{3}{2}} \right. \\ &\quad \left. - \frac{1}{3(at)^2} [(atk_c)^2 + \mathbb{B}_{\tau s}^2]^{\frac{3}{2}} \right\} \\ &= 3\mathbb{A}_{\tau s} k_c^2 (\tan(\varphi_m) - \varphi_m) - \frac{2}{(at)^2} \varphi_m \mathbb{C}_{\tau s}^3 \\ &\quad + 6\mathbb{D}_{\tau s}, \end{aligned} \quad (\text{C21})$$

where $\varphi_m = \arccos(k_c/k_F^{\tau s})$. $\mathbb{D}_{\tau s}$ denotes an integration

$$\mathbb{D}_{\tau s} = \frac{1}{3(at)^2} \int_0^{\varphi_m} d\varphi \left[\left(\frac{atk_c}{\cos(\varphi)} \right)^2 + \mathbb{B}_{\tau s}^2 \right]^{\frac{3}{2}}. \quad (\text{C22})$$

It is hard for $\mathbb{D}_{\tau s}$ to obtain an analytical formula. Therefore, $\mathbb{D}_{\tau s}$ is calculated numerically. When $k_c < k_F^{\tau s} \leq k_m$,

$$\begin{aligned} E_{\text{free}}^{\tau s} &= \frac{\pi}{3(at)^2} (3\mathbb{B}_{\tau s}^2 \mathbb{C}_{\tau s} - \mathbb{C}_{\tau s}^3 - 2\mathbb{B}_{\tau s}^3) + \pi k_c^2 \mathbb{E}_{\text{cts}}(k_c) \\ &\quad + \frac{\theta}{2(at)^2} (\mathbb{A}_{\tau s}^3 - 2\mathbb{B}_{\tau s}^3 - 3\mathbb{B}_{\tau s}^2 \mathbb{A}_{\tau s}) - \frac{3\theta}{2\pi} E_1^{\tau s} \\ &\quad + 3\mathbb{A}_{\tau s} k_c^2 (\tan(\varphi_m) - \varphi_m) - \frac{2}{(at)^2} \varphi_m \mathbb{C}_{\tau s}^3 \\ &\quad + 6\mathbb{D}_{\tau s}. \end{aligned} \quad (\text{C23})$$

As for $0 \leq k_F^{\tau s} \leq k_c$, the total free energy is obtained by substituting Eq. (C16) into Eq. (C15). For $k_c < k_F^{\tau s} \leq k_m$, the total free energy is calculated by substituting Eq. (C17) into Eq. (C15).

-
- [1] S. Manzeli, D. Ovchinnikov, D. Pasquier, O. V. Yazyev, and A. Kis, *Nat. Rev. Mater.* **2**, 17033 (2017).
- [2] K. F. Mak and J. Shan, *Nat. Photonics* **10**, 216 (2016).
- [3] Q. H. Wang, K. Kalantar-Zadeh, A. Kis, J. N. Coleman, and M. S. Strano, *Nat. Nanotechnol.* **7**, 699 (2012).
- [4] K. F. Mak, C. Lee, J. Hone, J. Shan, and T. F. Heinz, *Phys. Rev. Lett.* **105**, 136805 (2010).
- [5] J. A. Wilson and A. D. Yoffe, *Adv. Phys.* **18**, 193 (1969).
- [6] J. A. Wilson, F. J. D. Salvo, and S. Mahajan, *Phys. Rev. Lett.* **32**, 882 (1974).
- [7] M. M. Ugeda, A. J. Bradley, Y. Zhang, S. Onishi, Y. Chen, W. Ruan, C. Ojeda-Aristizabal, H. Ryu, M. T. Edmonds, H.-Z. Tsai, A. Riss, S.-K. Mo, D. Lee, A. Zettl, Z. Hussain, Z.-X. Shen, and M. F. Crommie, *Nat. Phys.* **12**, 92 (2016).
- [8] S. Bertolazzi, J. Brivio, and A. Kis, *ACS Nano* **5**, 9703 (2011).
- [9] B. Radisavljevic, A. Radenovic, J. Brivio, V. Giacometti, and A. Kis, *Nat. Nanotechnol.* **6**, 147 (2011).
- [10] S. Das, R. Gulotty, A. V. Sumant, and A. Roelofs, *Nano Lett.* **14**, 2861 (2014).
- [11] G. M. Marega, Y. Zhao, A. Avsar, Z. Wang, M. Tripathi, A. Radenovic, and A. Kis, *Nature (London)* **587**, 72 (2020).
- [12] N. Zibouche, P. Philippsen, A. Kuc, and T. Heine, *Phys. Rev. B* **90**, 125440 (2014).
- [13] D. Xiao, G.-B. Liu, W. Feng, X. Xu, and W. Yao, *Phys. Rev. Lett.* **108**, 196802 (2012).
- [14] H. Zeng, J. Dai, W. Yao, D. Xiao, and X. Cui, *Nat. Nanotechnol.* **7**, 490 (2012).
- [15] J. R. Schaibley, H. Yu, G. Clark, P. Rivera, J. S. Ross, K. L. Seyler, W. Yao, and X. Xu, *Nat. Rev. Mater.* **1**, 16055 (2016).

- [16] F. H. L. Koppens, T. Mueller, P. Avouris, A. C. Ferrari, M. S. Vitiello, and M. Polini, *Nat. Nanotechnol.* **9**, 780 (2014).
- [17] L. Wang, D. Xu, L. Jiang, J. Gao, Z. Tang, Y. Xu, X. Chen, and H. Zhang, *Adv. Funct. Mater.* **31**, 2004408 (2020).
- [18] A. Chernikov, T. C. Berkelbach, H. M. Hill, A. Rigosi, Y. Li, O. B. Aslan, D. R. Reichman, M. S. Hybertsen, and T. F. Heinz, *Phys. Rev. Lett.* **113**, 076802 (2014).
- [19] P. Back, M. Sidler, O. Cotlet, A. Srivastava, N. Takemura, M. Kroner, and A. Imamoğlu, *Phys. Rev. Lett.* **118**, 237404 (2017).
- [20] J. Shang, X. Shen, C. Cong, N. Peimyoo, B. Cao, M. Eginligil, and T. Yu, *ACS Nano* **9**, 647 (2015).
- [21] Y. You, X.-X. Zhang, T. C. Berkelbach, M. S. Hybertsen, D. R. Reichman, and T. F. Heinz, *Nat. Phys.* **11**, 477 (2015).
- [22] Z. Wang, K. F. Mak, and J. Shan, *Phys. Rev. Lett.* **120**, 066402 (2018).
- [23] H. C. P. Movva, B. Fallahazad, K. Kim, S. Larentis, T. Taniguchi, K. Watanabe, S. K. Banerjee, and E. Tutuc, *Phys. Rev. Lett.* **118**, 247701 (2017).
- [24] J. G. Roch, G. Froehlicher, N. Leisgang, P. Makk, K. Watanabe, T. Taniguchi, and R. J. Warburton, *Nat. Nanotechnol.* **14**, 432 (2019).
- [25] J. G. Roch, D. Miserev, G. Froehlicher, N. Leisgang, L. Sponfeldner, K. Watanabe, T. Taniguchi, J. Klinovaja, D. Loss, and R. J. Warburton, *Phys. Rev. Lett.* **124**, 187602 (2020).
- [26] H. Dery, *Phys. Rev. B* **94**, 075421 (2016).
- [27] D. Miserev, J. Klinovaja, and D. Loss, *Phys. Rev. B* **100**, 014428 (2019).
- [28] M. Van der Donck and F. M. Peeters, *Phys. Rev. B* **98**, 115432 (2018).
- [29] J. E. H. Braz, B. Amorim, and E. V. Castro, *Phys. Rev. B* **98**, 161406(R) (2018).
- [30] E. S. Kadantsev and P. Hawrylak, *Solid State Commun.* **152**, 909 (2012).
- [31] In our model Hamiltonian, we merely consider two conduction and valence bands. Since the band edges of conduction and valence bands are renormalized by electron Coulomb interaction and shifted from those in the noninteracting case, the chemical potentials studied in this paper for various figures are finally not lying deeply in the conduction band after the renormalization. In this sense, the effect of more bands with higher energies cannot play an important role in this study. Moreover, we believe that the strong electron-electron interaction at low electron density plays a determining role in the ferromagnetic ground state. The high chemical potential leads to more occupied conduction bands and high electron density [30], which can't change the phase transition discussed in this paper.
- [32] X.-Q. Yu, Z.-G. Zhu, G. Su, and A.-P. Jauho, *Phys. Rev. Lett.* **115**, 246601 (2015).
- [33] H. Bruus and K. Flensberg, *Many-Body Quantum Theory in Condensed Matter Physics: An Introduction* (Oxford University, Oxford, 2004).
- [34] R. Roldán, E. Cappelluti, and F. Guinea, *Phys. Rev. B* **88**, 054515 (2013).
- [35] H. Rostami and R. Asgari, *Phys. Rev. B* **91**, 235301 (2015).
- [36] Z. Song, Z. Li, H. Wang, X. Bai, W. Wang, H. Du, S. Liu, C. Wang, J. Han, Y. Yang, Z. Liu, J. Lu, Z. Fang, and J. Yang, *Nano Lett.* **17**, 2079 (2017).
- [37] L. V. Keldysh, *Sov. J. Exp. Theor. Phys. Lett.* **29**, 658 (1979).